Hydrogen-Evolution Reaction

DOI: 10.1002/anie.201407031

Advancing the Electrochemistry of the Hydrogen-Evolution Reaction through Combining Experiment and Theory

*Yao Zheng, Yan Jiao, Mietek Jaroniec, and Shi Zhang Qiao**

density-functional theory · electrocatalysis · hydrogen-evolution reaction · mechanistic studies

The electrocatalytic hydrogen-evolution reaction (HER), as the main step of water splitting and the cornerstone of exploring the mechanism of other multi-electron transfer electrochemical processes, is the subject of extensive studies. A large number of high-performance electrocatalysts have been developed for HER accompanied by recent significant advances in exploring its electrochemical nature. Herein we present a critical appraisal of both theoretical and experimental studies of HER electrocatalysts with special emphasis on the electronic structure, surface (electro)chemistry, and molecular design. It addresses the importance of correlating theoretical calculations and electrochemical measurements toward better understanding of HER electrocatalysis at the atomic level. Fundamental concepts in the computational quantum chemistry and its relation to experimental electrochemistry are also presented along with some featured examples.

1. Introduction

The global demand for energy increased rapidly and continuously during the last few decades. Meanwhile, many advanced technologies for clean and renewable energy conversion, such as water electrolysis and fuel cells attract growing attention owing to the dwindling petroleum supplies.[1] Hydrogen, as a key energy carrier, plays a significant role in these two technologies: the electrocatalytic hydrogen-evolution reaction (HER) is a cathodic reaction in the electrolysis of water, while its reverse reaction, the hydrogen-oxidation reaction (HOR) is the anodic reaction in fuel cells. Although detailed investigations of the HER kinetics on the surfaces of solid electrodes have a long history,[2] the recent rapid developments in the computational quantum chemistry and experimental nanotechnology, and especially their successful merger, have brought some new insights into the electrochemistry of HER at both fundamental and utilization levels.[3]

The most popular HER electrocatalyst is platinum (Pt), which exhibits extremely high exchange current density (j_0) and small Tafel slope.[4] However, the major drawbacks of Pt catalysts are their high cost and insufficient Pt reserves. To assure a sustainable hydrogen production, the cost-effective alternatives to precious Pt featuring high electrocatalytic activities and robust stabilities should be developed. Experimentally, a large number of candidates have been fabricated as a result of significant advances in synthetic chemistry. For example, various earth-abundant transition metals (Fe, Co, Ni, Mo) and their compounds have been designed and developed as highly efficient HER electrocatalysts under either acidic or alkaline conditions.[5] Accurate identification of HER active sites on these electrocatalysts and remarkable advances in nanotechnology jointly promoted the development of numerous nanostructured electrocatalysts with preferentially exposed active sites and great performances.[6] Strikingly, some non-metallic carbon-based materials with unique electronic properties have been also considered as innovative alternatives for Pt catalyst.[7] The availability of various carbon nanostructures (fullerenes, carbon nanotubes, graphene, and hybrids) with tunable composition (heteroa-

[*] Dr. Y. Zheng,[+] Dr. Y. Jiao,[+] Prof. S. Z. Qiao
School of Chemical Engineering
University of Adelaide
Adelaide, SA 5005 (Australia)
E-mail: s.qiao@adelaide.edu.au
Prof. M. Jaroniec
Department of Chemistry and Biochemistry, Kent State University
Kent, OH 44240 (USA)
[+] These authors contributed equally to this work.

tom dopants) significantly enlarged the number of candidates for highly efficient HER.

In parallel to the development of experimental strategies, quantum chemistry studies that take into account the surface (electro)chemistry and electronic structure of solid electrodes have been essential for improving the fundamental understanding of HER electrocatalysis. Extraordinary progress in density functional theory (DFT) has created enormous possibilities in the computer-aided design of catalysts with most favorable activity. Some theoretical concepts, such as "adsorption free energy", "microkinetic models", "volcano plots", and "d-band centers" have also been widely used for (semi)quantitative evaluation of the performance of synthesized HER electrocatalysts. Importantly, the origin of the electrocatalytic reactivity of solid electrodes could be uncovered by analyzing certain activity descriptors derived on the basis of DFT calculations, paving the way to the molecular design of more efficient candidates for HER and other related electrocatalytic processes.[3b]

At present, there are tremendous opportunities in advancing electrochemical surface science at the atomic/molecular level by merging computational and experimental methodologies, which leads to many breakthroughs in the research and development of HER electrocatalysts. For example, the most advanced spectroscopic tools are capable of elucidating the chemical/electronic properties of solid surfaces predicted by computational quantum chemistry,[8] while cutting-edge nanotechnologies ensure the design-driven fabrication of catalysts with tunable surface properties as projected by theoretical models.[9] Herein, we highlight recent advances in the merging of fundamental science and technology to promote the electrochemical studies of HER. In particular, our intention is to show how computational chemistry could be used to direct the proof-of-concept molecular design of highly active electrocatalysts, and how electrochemical experiments can be used to verify theoretical predictions. The main aim of this Minireview is to provide a comprehensive account, addressing both computational and experimental aspects of HER, toward better/deeper understanding electrochemistry of this process.

2. Electrocatalytic Activity: Theoretical Descriptors and Trends

2.1. Fundamentals of HER

2.1.1. Reaction Mechanism

HER ($2H^+ + 2e^- \rightarrow H_2$) is a multi-step electrochemical process taking place on the surface of an electrode that generates gaseous hydrogen. Generally accepted reaction mechanisms in acid and alkaline solutions are:[10]

1) electrochemical hydrogen adsorption (Volmer reaction) [Eq. (a),(b)]

$$H^+ + M + e^- \rightleftharpoons M{-}H^* \text{ (acid solution)} \quad \text{(a)}$$

$$H_2O + M + e^- \rightleftharpoons M{-}H^* + OH^- \text{ (alkaline solution)} \quad \text{(b)}$$

followed by

Yao Zheng received his Ph.D. in 2014 from the University of Queensland (Australia) in the group of Prof. Shi Zhang Qiao. Currently he is a postdoctoral researcher in University of Adelaide working with Professor Shi Zhang Qiao. His research focuses on developing cost-effective alternatives to precious-metal catalysts for key electrocatalysis processes, such as oxygen reduction, hydrogen evolution, and CO_2 reduction reactions.

Mietek Jaroniec received his Ph.D. from M. Curie-Sklodowska University (Poland) in 1976; he was appointed as a faculty at the same University. Since 1991, he is Professor of Chemistry at Kent State University, Kent, Ohio (USA). His research interests include interfacial chemistry and chemistry of materials, especially adsorption at the gas/solid and liquid/solid interfaces and nanoporous materials. He is also interested in ordered mesoporous silicas, organosilicas, inorganic oxides, carbons, and nanostructured catalysts/photocatalysts, focusing on their synthesis, characterization and environmental and energy-related applications.

Yan Jiao received her Ph.D. in 2012 from the University of Queensland in the group of Prof. John Zhu. She is currently a postdoctoral researcher in the University of Adelaide working with Professor Shi Zhang Qiao. Her current research focuses on discovering the electronic-structure origin of electrocatalytic activity in carbon-based materials, and engineering novel carbon-based catalysts for clean energy conversion reactions.

Shi Zhang Qiao received his Ph.D. in chemical engineering from Hong Kong University of Science and Technology in 2000, and is currently a Chair Professor at School of Chemical Engineering of The University of Adelaide, Australia. His research expertise is in nanomaterials and nanoporous materials for drug/gene delivery and new energy technologies. He has be honored with the ARC Discovery Outstanding Researcher Award (2013), Emerging Researcher Award (2013, ENFL Division of the American Chemical Society), ARC ARF and APD Fellowships.

2) electrochemical desorption (Heyrovsky reaction) [Eq. (c),(d)]

$$M{-}H^* + H^+ + e^- \rightleftharpoons M + H_2 \text{ (acid solution)} \quad (c)$$

$$M{-}H^* + H_2O + e^- \rightleftharpoons M + OH^- + H_2 \text{ (alkaline solution)} \quad (d)$$

or

3) chemical desorption (Tafel reaction) [Eq. (e)]

$$2\,M{-}H^* \rightleftharpoons 2\,M + H_2 \text{ (both acid and alkaline solutions)} \quad (e)$$

where H* designates a hydrogen atom chemically adsorbed on an active site of the electrode surface (M).

These pathways are strongly dependent on the inherent (electro)chemical and electronic properties of the electrode surface.[3c,4,9] The determination of reactions (1), (2) or (3) as the possible rate-controlling steps can be simply discerned by evaluating the Tafel slope value from the HER polarization curve as it was carefully explained by Conway and Tilak.[4]

As indicated by reactions (1) and (2)/(3), chemical adsorption and desorption of H atoms on an electrode surface are competitive processes. According to the Sabatier principle,[11] a good HER catalyst should form a sufficiently strong bond with adsorbed H* for facilitating the proton-electron-transfer process, but it should be also weak enough to assure a facile bond breaking and the release of gaseous H_2 product. However, the establishment of quantitative relationships between the energetics of the H* intermediate and the HER electrochemical reaction rate is difficult owing to the absence of directly measured values for the surface-intermediate bonding energy.[8] From the physical chemistry perspective, the free energy change for H* adsorption on a catalyst surface (ΔG_H*) can be used to evaluate both H* adsorption and H_2 desorption by means of the HER free energy diagram.[12] According to Sabatier principle, ΔG_H* should be zero, under this condition the overall reaction has the maximum rate (expressed in terms of HER exchange current density, j_0). More importantly, a close correlation has been proposed between the experimental j_0 value and the quantum chemistry-derived ΔG_H* in the form of a "volcano curve" for a wide variety of electrode surfaces.[2b,12] Guided by this trend, the relationship between the electrochemical nature of a solid surface and HER kinetics could be principally established. In the following Sections, we attempt to give some insights into the relationship between j_0 and ΔG_H*, and to discuss its essential role toward design of HER electrocatalysts.

2.1.2. Exchange Current Density and Micro-kinetic Modelling

The term j_0 is the key descriptor of the electrocatalyst's activity, which profoundly affects the total electrochemical reaction rate. Physically, it is defined as the current density in one direction at one reaction's equilibrium potential (U^0, 0 V versus the standard hydrogen electrode (SHE) for HER). Then, the forward and backward reaction rates near U^0 can be expressed by Equations (1),(2)[13]

$$j_{forward} = -j_0 \exp(-\alpha_c F\eta/RT) \quad (1)$$

$$j_{backward} = j_0 \exp(\alpha_a F\eta/RT) \quad (2)$$

where α_c and α_a are the cathodic and anodic charge-transfer coefficients ranging from 0 to 1. Under a certain overpotential (η), the overall electrode current density (j) can be represented by the Butler–Volmer equation as [Eq. (3)]:

$$j = j_{forward} + j_{backward} \quad (3)$$

According to the micro-kinetic model, j_0 can be theoretically computed as an indirect function of ΔG_H* [Eq. (4)][12]

$$j_0 = F\,k^0\,C_{total}[(1-\theta)^{1-\alpha}\,\theta^{\alpha}] \quad (4)$$

where k^0 is the standard rate constant, which was experimentally determined for a Pt surface to be 200 s^{-1} $site^{-1}$, and it is widely applied for other types of surfaces.[12] C_{total} is the total number of HER active sites on the electrode surface. The percentage coverage for H* intermediate on the surface, θ, is normally related to the H* heat of adsorption corresponding to the Langmuir adsorption model [Eq. (5)]:

$$\theta = (1+K)/K \quad (5)$$

where K is the equilibrium constant, defined as the value of the reaction quotient at thermodynamic equilibrium, and can be expressed as a function of ΔG_{H^*} [Eq. (6)]:[12]

$$K = \exp(-\Delta G_{H*}/k_B T) \quad (6)$$

where k_B is the Boltzmann constant. By relating Equations (4) to (6), a volcano-shaped curve that associates the macroscopic j_0 as a function of microscopic ΔG_{H^*} can be quantitatively established. This intrinsic relationship has been verified to be widely applicable for various types of surfaces (single-crystal metal, alloy, metal compounds, and carbon-based materials) and the calculated activity trends agree well with experimental data (see Section 3.3 for details).

2.2. Density Functional Theory (DFT) in Electrocatalysis

2.2.1. Standard Free Energy Change Calculation

As mentioned in the preceding Sections, ΔG_{H^*} is one of the key descriptors in theoretical prediction of the activity for HER on solid electrodes. The development of computational quantum chemistry provides a feasible methodology to calculate the value ΔG_{H^*} by modelling the possible intermediates formed during hydrogen adsorption–reduction–desorption processes and evaluating their stabilities on the electrode surface [Eq. (7)]:[12]

$$\Delta G_{H*} = \Delta E_{H*} + \Delta E_{ZPE} - T\Delta S \quad (7)$$

where ΔE_{H^*} can be calculated by taking the separated H_2 as a reference state [Eq. (8)]:

$$\Delta E_{H*} = E_{(surface+H*)} - E_{(surface)} - 1/2\,E_{H2} \quad (8)$$

The zero-point energy change (ΔE_{ZPE}) for adsorbed H* and isolated H_2 could be obtained by vibrational frequency calculation [Eq. (9)]:[14]

$$\Delta E_{ZPE} = 1/2\,\Sigma h\nu_i \quad (9)$$

where ν_i are the computed vibrational frequencies. The entropy change (ΔS) in Equation (7) could be obtained as [Eq. (10)]:

$$S = S_{trans} + S_{vib} + S_{rot} + S_{el} \quad (10)$$

where S_{trans}, S_{vib}, S_{rot}, and S_{el} are the translational, vibrational, rotational, and electronic entropy terms that can be derived by frequency calculations.[14] It should be noted that although it is a simplified model, the ΔG_{H^*} value can give a high level of accuracy to favorably compare experimental results.[3b]

2.2.2. The d-Band Theory for HER

As presented in Ref. [12], the calculation of ΔG_{H^*} is mainly related to the electronic structure of a solid surface. DFT calculations can also offer a closer view on how the inherent electronic structure, especially the metal d-orbital levels, would affect the strength of H* adsorption on the surface of a given electrode. The d-band center (ε_d, normally defined as the central position of the d-orbitals) theories were developed, either by considering the adsorbed H* state by itself,[15] or taking into account the energy-level realignment during the bond breaking in HER process.[16] Considering the adsorbed H* state by itself, when H* adsorbs on a transition-metal surface, the metal d-orbital electrons contribute mostly to the metal–H bond formation (Figure 1 a).[15] Additionally, the hybridization of the H* orbital with the metal d-orbital results in a low-energy, fully filled bonding orbital (σ) and a high-energy, partially filled anti-bonding orbital (σ*), in which the occupancy of the anti-bonding orbital determines the metal–H bonding strength (the lower σ* occupancy, the higher bonding strength). Qualitatively, Ni(111) and Pt(111) show unfilled σ* states with a strong hydrogen adsorption ($\Delta G_H^* < 0$); while in the case of Au(111) and Cu(111), the energies of the σ* states are below Fermi energy (filled), resulting in relative weak hydrogen adsorption ($\Delta G_H^* > 0$) (Figure 1 b).[17] Thus, by computing the local d-band states of a metal surface, its adsorbing ability toward hydrogen can be qualitatively described and predicted. Basically, if the d-band center is closer to the metal's Fermi level (i.e. higher), the resultant σ* level is higher (reduced σ* occupancy), which corresponds to a stronger H* adsorption.[17] Besides adsorbed H* state, Santos et al. investigated the influence of d-band position on the bond breaking barrier and electron transfer process in HER (Figure 1 c).[16a] It was suggested that the d-orbital position and occupancy is more important for the bond-breaking saddle point, than for the H* adsorption on the surface. Based on this assumption, it was calculated that when ε_d is at the Fermi level, the activation barrier for the bond breaking is the lowest (Figure 1 d).[16a] This conclusion was derived on the basis of molecular binding using Hückel

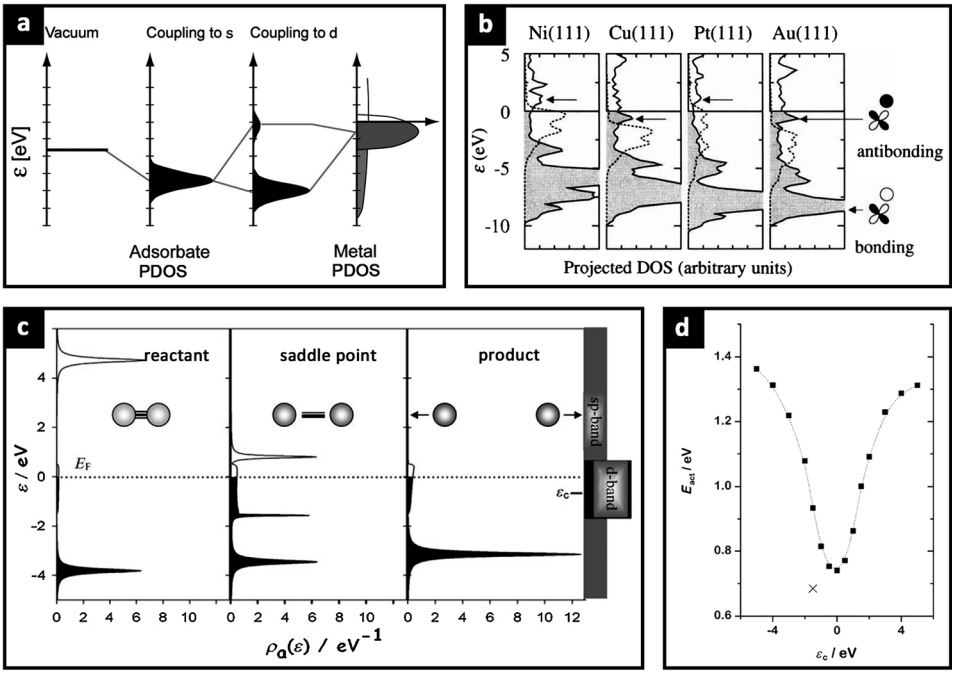

Figure 1. a) Schematic illustration of the energy-level hybridization and realignment for chemical-bond formation between an adsorbate and a transition-metal surface. Reproduced with permission from Ref. [15]. Copyright 2005, Springer. b) The projected DOS for atomic hydrogen chemisorbed on the (111) face of Ni, Cu, Pt, and Au. Dashed lines show the surface DOS of clean metals. Reproduced with permission from Ref. [17]. Copyright 1995, NPG. c) DOS at equilibrium for the H_2molecule, saddle point, and after bond breaking. d) The activation energy for the H_2molecule bond breaking as a function of the position of ε_d. (c, d) are reproduced with permission from Ref. [16a]. Copyright 2006, Wiley-VCH.

theory, and could be extended to real systems as suggested in Ref. [16b].

It should be noted that the above mentioned d-band theories refer to transition-metal surfaces, in which the d-orbitals play an important role in surface catalytic reactions as a result of their relatively close position to the Fermi level. Recently, the concept of metal-free catalysis started to emerge, such as carbon-based materials for various energy-related electrocatalytic reactions.[18] The trend of H* adsorption on different graphene surfaces and their valence-band orbital levels have been established by cluster model DFT calculations.[7b] It has been demonstrated that with increasing valence-band energy level, the H* adsorption strength decreases, which is interestingly contrary to the trend that has been observed on metal surfaces. This difference could be explained by the fact that in the graphene-H system, the graphene cluster's Fermi level does not cross the σ* orbital as in the case of metals, instead it crosses the σ orbital. With the downshifting of the valence orbitals, the σ orbital downshifts, leading to an increased filling (enhanced H* adsorption strength). This difference could probably be attributed to the different energy level of H bonding on different surfaces. For the graphene surface, the projected density of states (P-DOS) for H is mainly distributed near the Fermi level,[19] while for d-metals, such as Pt, they are buried deeper and far away from the Fermi level.[20]

2.3. HER Free-Energy Diagram

To present the possible extra reaction-rate limiting steps that have been ignored in calculating the ΔG_{H^*} descriptor, the reaction free-energy diagrams were proposed for both HER mechanisms (Volmer–Heyrovsky and Volmer–Tafel) on different types of surfaces including precious metals,[21] transition metals,[22] and non-metallic materials.[7a] The calculation of the explicit free-energy diagram could be quite complicated: the basis is the ΔG_{H^*} computation, but there are several extra factors that need to be considered, such as the solvation and electric-double-layer effects.[23] In addition to the free-energy level of each reaction step (reactant, intermediates, and final product), the possible reaction barriers can also affect the overall reaction rate (Figure 2). The calculation of reaction barriers for the Tafel step at both U^0 and certain η are achievable just by including $-ne \times \eta$ for each step (n denotes the electron numbers carried by the electrode surface and η is the overpotential of the electrode).[21a] However, for Volmer and Heyrovsky steps, the electrons carried by corresponding initial and final states are unbalanced thus it is impossible to obtain the barrier value by traditional DFT calculations. To address this issue, Nørskov et al. developed an two-step extrapolation scheme that could derive the barrier values under different η by i) introducing different proton numbers in the first water layer to model the surface under different η, and ii) calculating the barrier values for a series of selected unit cell sizes, and extrapolating the results to the limit of an infinitely large unit cell where the potential change of the surface induced by proton transfer is equal to zero.[21]

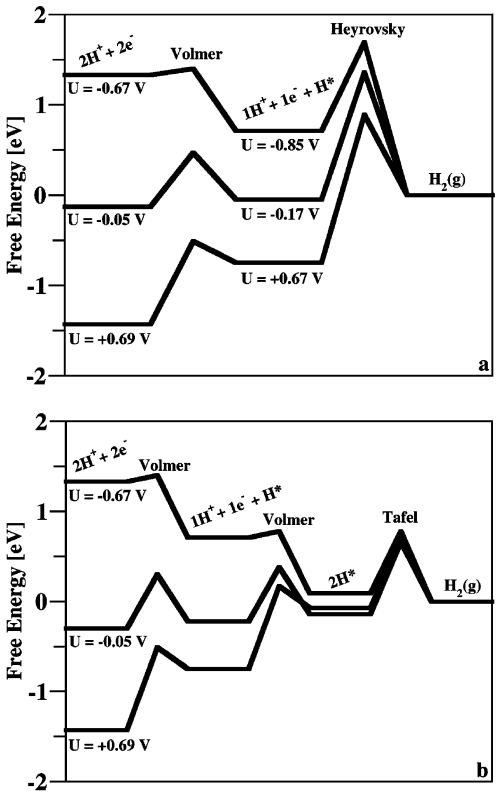

Figure 2. Standard HER free-energy diagram for the Volmer–Heyrovsky route (a) and Volmer–Tafel route (b) on Pt(111) under different overpotentials. Reproduced with permission from Ref. [21a]. Copyright 2010, ACS.

3. Combining Theory and Experiment for Predicting and Interpreting HER Activity

3.1. Identification of Active Sites

In general, monitoring the reaction intermediates formed on the surface of a catalyst represents a possible platform for exploring its catalytically active sites. However, it is difficult to observe in-situ these adsorbed species on a given site owing to their extremely short lifetimes.[24] Additionally, most experimental insights about the reaction mechanism have been inferred from rate measurements; unfortunately such procedures typically cannot provide conclusive evidence for a given mechanism since the measured rate of each reaction depends on several elementary steps and possible reaction barriers as discussed in Section 2.3.[21] Gratifyingly, the combination of theoretical modelling with advanced spectroscopic techniques and electrochemical measurements provides a feasible methodology to identify the intermediates and active sites on an electrode surface.[8]

3.1.1. Pt Single Crystal

Studies of HER/HOR on Pt ($h\ k\ l$) single-crystal surfaces date back to the early 1970s, and hydrogen adsorption was considered as one of the first adsorption systems studied with modern ultrahigh vacuum (UHV) surface-science tech-

niques.[8] Detailed HER kinetics on a Pt single crystal in both acidic and alkaline solutions have been studied by Marković et al.[25a,b] and Conway et al.[25c,d] They also proposed some key factors that influence the apparent HER current densities, such as roles of underpotential/overpotential-deposited hydrogen (H_{UPD} and H_{OPD}) and hydrogen coverage (θ_H) on the active sites. The subsequent calculations confirmed that HER on Pt (*h k l*) is indeed a structure-sensitive reaction and the activity is strongly related to the value of θ_H on different facets.[21a,25e] Since there are several excellent Reviews elsewhere providing overviews about the specificity of the HER kinetics to single-crystal Pt surfaces[3c,4,8] while similar studies on other single-crystal metal surfaces are limited, we will not discuss details of these kinds of materials herein.

3.1.2. The Importance of MoS_2 Edge

MoS_2 has also been considered as a potential HER electrocatalyst since 1970s.[26] However, only after a series of computational and experimental studies in the last decade, which led to the identification of its electrochemically active sites toward HER, is there a growing interest in this material as a competitive Pt alternative. The DFT calculations in terms of the HER free-energy diagram predict that only the edges of S-Mo-S in the MoS_2 domain sheet are active for H* adsorption, while the whole basal plane is electrocatalytically inert; in particular, the [1010] Mo edges are mainly responsible for bringing ΔG_{H^*} very close to that observed on Pt surfaces and much more favorable than other transition metals (Figure 3a).[27] The verification of this theoretical conclusion by electrochemical measurements and scanning tunneling microscopy (STM) imaging demonstrated that j_0 measured on MoS_2 nanoplatelets supported on Au (111) is proportional to the length of the edge sites (obtained from the observation by STM), but irrelative to the whole exposed area of MoS_2 nanoplatelets (Figure 3b);[28] the agreement between theory and experiment is remarkably good.

3.1.3. Various Methods of MoS_2 Edge Engineering

Confirmation of the catalytic activity of MoS_2 edges in HER was essential for developing various nanoengineering strategies for the preparation of MoS_2 nanomaterials with exposed/extended active edge sites. The physical and surface properties of pristine MoS_2 could also be modified by morphological changes as it was shown elsewhere.[6c] The earliest and most popular strategy involves the enlargement of MoS_2 surface area by fabricating different nanostructures, such as mesostructures (Figure 4a),[29] nanowires,[30] nanoporous objects,[31] nanosheets,[32] and nanoparticles.[33] This approach does not alter the electronic properties of pristine MoS_2 but can physically increase the number or fraction of electrocatalytically active sites per unit geometric area of the electrode to enhance the apparent HER current density. Different from simple nanostructuring, chemical exfoliation of bulk MoS_2 or WS_2 to nanosheet forms is also an effective way to not only achieve a high density of exposed active edges, but to tailor their electronic structure by transforming the material from the semiconducting 2H (trigonal prismatic)

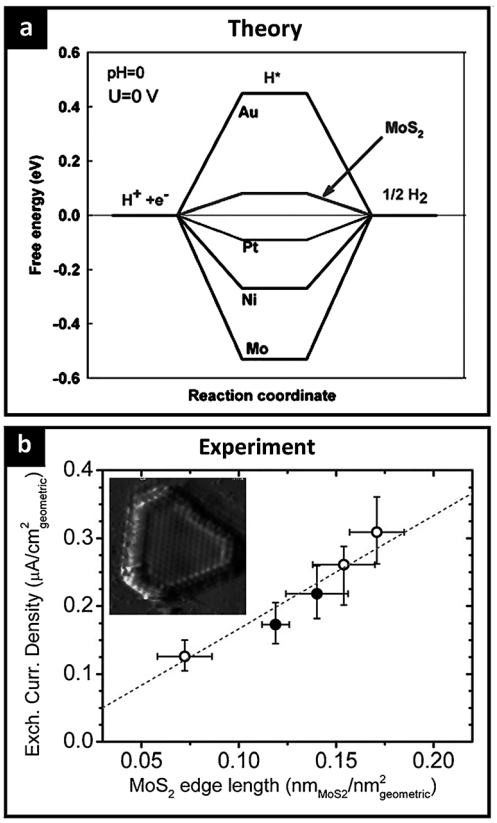

Figure 3. a) Calculated HER free-energy diagram for MoS_2 and different metals. Reproduced with permission from Ref. [27]. Copyright 2005, ACS. b) The relationship of j_0 with the MoS_2 nanoplatelet edge length measured from STM images as shown in the inset. Reproduced with permission from Ref. [28]. Copyright 2007, AAAS.

to the metallic 1T (octahedral) phase (Figure 4b).[34] The experimentally observed high activity of 1T-MoS_2 nanosheets is mostly attributed to the intrinsic facile electrode kinetics and low-loss in electron transport rather than the proliferation of active sites.[34] In the case of the exfoliated WS_2 nanosheets, which underwent the transformation from the 2H to 1T phase, the structure became highly distorted with a high proportion of zigzag-like strains in the lattice.[35] The DFT calculations showed that these tensile strains could significantly influence ΔG_{H^*} by enhancing the density of states near WS_2's Fermi level, which is also consistent with the electrochemical observations indicating that the measured j_0 is closely related to 1T phase concentration and strain in the exfoliated WS_2 nanosheets.[35]

Although electron transport on the catalyst's surface is a separate process from the charge-transfer reactions involved in the electrocatalytic HER process, it affects the overall activity of a catalyst and is often reflected by high Tafel slopes.[6a] Thus, engineering semiconductive MoS_2 with conductive templates or supports (graphene,[36] carbon nanotube[37] and both[38]) was proposed to improve the catalytic activity of the host material. Importantly, in addition to the enhanced electron-transfer capability of a nanocarbon support, the coupling/interaction of MoS_2 with the support could lead to a selective growth of highly dispersed MoS_2 nano-

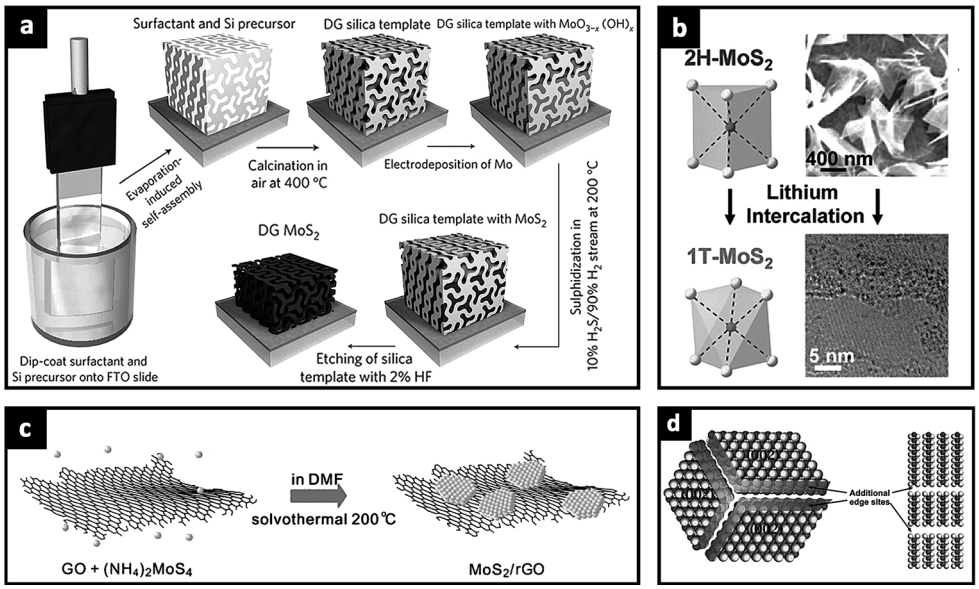

Figure 4. a) Synthesis procedure and nanostructural model for mesoporous MoS_2 with a double-gyroid morphology. Reproduced with permission from Ref. [29]. Copyright 2012, NPG. b) Molecular models of exfoliation inducing a phase transition from 2H- to 1T-MoS_2 and SEM/TEM images of the material. Reproduced with permission from Ref. [34]. Copyright 2013, ACS. c) Solvothermal synthesis of MoS_2 on reduced graphene oxide (rGO). Reproduced with permission from Ref. [36a]. Copyright 2011, ACS. d) Atomic reconstruction of defect-rich MoS_2 with additional active edges as indicated by the arrows. Reproduced with permission from Ref. [40]. Copyright 2013, Wiley-VCH.

particles with favorably exposed active sites. For example, MoS_2 supported on chemically reduced graphene oxide (rGO; Figure 4c) showed a significantly higher HER activity than the free-standing bulk sample under the same conditions.[36a] Hydrogen adsorption free-energy calculations showed that Mo-edges that exhibit a strong adhesion to the support (e.g. graphene) can weaken the hydrogen binding and optimize ΔG_{H^*} on the active edge of MoS_2,[39] revealing the function of the carbon support in HER at the atomic level and also providing a rigorous theoretical reasoning of the high performance of MoS_2/carbon hybrids.

Intramolecular self-generated active sites in the MoS_2 framework were also considered and deliberately formed by synthesizing defect-rich MoS_2 ultrathin nanosheets, which are prone to partial cracking along the basal planes to form nanosized domains leading to the exposure of additional active edge sites (Figure 4d).[40] The remaining periodicity (sixfold symmetry) partially retains the electron conjugation on S-Mo-S layers, leading to a favorable internal conductivity. Consequently, the HER performance on the defect-rich MoS_2 is dramatically enhanced compared to the defect-free nanosheets as a result of the synergistic effect of the newly generated active edge sites and nanosheet morphology.[40] Considering the decreased interdomain conductivity arising from the abundant defects, Xie et al. incorporated oxygen into MoS_2 framework to give controllable disorder.[41] Theoretical analysis showed that the disordered structure can offer abundant unsaturated sulfur atoms as active sites for hydrogen adsorption, while the oxygen incorporation can reduce MoS_2's band gap to improve its intrinsic conductivity.[41] Driven by these effects, the oxygen-MoS_2 nanosheets demonstrated a better activity than pure and bulk samples.

3.2. Correlation between Electronic Structure and Surface Properties

As discussed in Section 2.2.2, there is a close correlation between the catalyst's electronic structure (e.g. d-band center or valence orbital position) and its surface (electro)chemical properties. By tailoring the electronic structure of a solid electrode, in principle, the binding energy of reactant on the catalyst surface can be optimized to facilitate the whole catalytic process.[42] DFT shows its powerful capability for describing the electronic structures of catalysts, while variations in the d-band center for a given metal can be achieved by measuring the surface core-level shifts or by using valence-band photoelectron spectroscopy.[43] By the combination of theory and experiments, we present three typical strategies for the design of highly efficient HER electrocatalysts through electronic structure engineering.

3.2.1. Bimetallic Systems

Introducing another element into the lattice of a given metal is an effective way to modify its electronic/chemical properties by creating a bimetallic surface through: i) formation of heteroatom bonds leading to a ligand effect, and ii) alteration of the average metal–metal bond length, resulting in a strain (e.g. compressive or tensile) effect.[44] Individual contributions of the ligand and strain effects to the shifts in the metal's d-band center were theoretically calculated and found to correlate with the optimized ΔG_{H^*}.[45] For example, the Pt surface's d-band can be broadened and lowered in energy by interacting with subsurface 3d metals resulting in weaker dissociative adsorption energies of hydrogen on these

surfaces.[46] The choice of the secondary metal could be achieved by a computational screening procedure, which is an efficient approach to semiquantitative identification of a large number of potential candidates by evaluating some special selection criteria.[46] Considering the stability of bimetals, Greeley et al. theoretically identified one couple of interesting candidates (Bi and Pt) from over 700 binary surface alloy samples (Figure 5a). As expected, the carefully synthesized Bi supported on Pt surface alloy (by underpotential deposition followed by annealing) indeed demonstrated an enhanced HER activity compared to pure Pt (Figure 5b),[46] although Bi itself is a notoriously poor electrocatalyst for HER. Guided by this success, Bjorketun et al. further extended the choice of alloys to non-precious metals (W–Cu alloy nanoparticles) by using a computational screening selection procedure.[47] Importantly, such a strategy has also been applied in other key electrocatalytic processes, such as the oxygen-reduction reaction (ORR)[48] and electrochemical H_2O_2 production[49] by decorating Pt with 3d metals. The experimentally measured activities of DFT-designed electrocatalysts were better than that of pure Pt.

In addition to Pt, systematic studies regarding the deposition of pseudomorphic Pd monolayers onto noble-metal substrates also revealed that the hydrogen adsorption strength on a solid surface can be significantly influenced by its electronic properties. Depending on the lattice parameters of the substrate, the deposited Pd overlayer is either compressed or expanded. Hammer and Nørskov theoretically pointed out that an expanded monolayer can lead to an upshift of the d-band center owing to the band narrowing and energy conservation.[50] To verify this prediction, Kibler et al.[51] and Greeley et al.[43a] separately prepared pseudomorphic Pd monolayers on a wide variety of single-crystal noble metals with different geometric characters (both hexagonally close-packed and face-centered cubic, such as Au(111), Re(0001), Ru(0001), Rh(111), Ir(111), Pt/Ru (111), and Pt(111)) by underpotential deposition. A comparison of the electrochemical performance of these systems demonstrated that there is a close correlation between the apparent H* binding strength on the decorated Pd overlayer with the calculated shift of the d-band center induced by lateral strain or ligand effect in bimetallic systems (the higher the energy of the d-states, the stronger the bonds that are formed between H* and the surface, as shown in Figure 5c,d). These findings agree very well with the d-band center theory discussed in Section 2.2.2. Maark and Peterson[52] concluded that the strain gives a systematic contribution to the binding-energy changes, while the ligand effect can act to either intensify or weaken the strain effect. For some systems (e.g. Pd/Ir), the ligand effect is more pronounced than the strain effect while in others (e.g. Pd/Au) the strain effect is more significant.

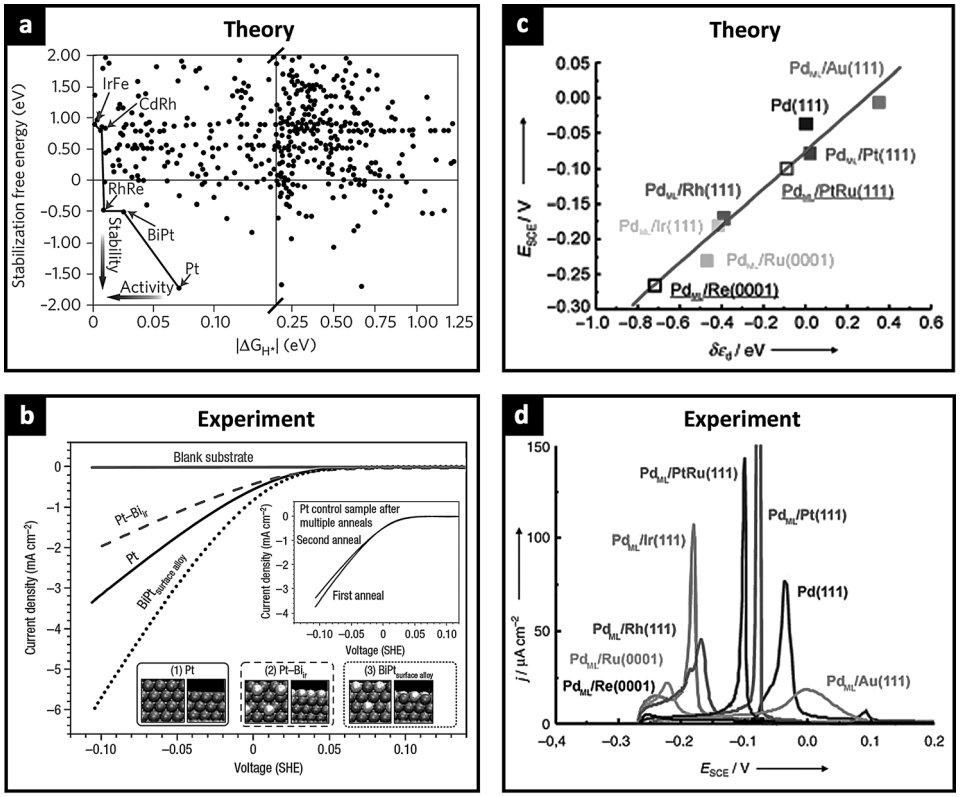

Figure 5. a) DFT calculation-derived stability of different surface alloys plotted as a function of ΔG_{H^*}. b) HER polarization curves of various Pt-based electrocatalysts. Reproduced with permission from Ref. [46]. Copyright 2009, NPG. c) A plot of the hydrogen-desorption potentials versus the shift of the d-band center. d) Positive voltammetric sweeps for Pd(111) and pseudomorphic Pd monolayers (Pd_{ML}) on seven different single-crystal substrates in 0.1 M H_2SO_4. Reproduced with permission from Ref. [51]. Copyright 2005, Wiley-VCH.

3.2.2. Promoted MoS_2 Edge

The modification of electronic structure can also be achieved by doping another element into a metal compound. The most pronounced example is doping MoS_2 with Co and Ni for the catalytic hydrosulfurization reaction.[53] The promotion effect can be theoretically explored by projected DOS analysis showing that Co or Ni can weaken the bonding of S at the S-edges owing to an increased filling of the antibonding state (Figure 6a).[54] Consequently, some coordinatively unsaturated metal atoms are created, which can interact with adsorbates. Quantitatively, HER on MoS_2 is expected to take place predominantly at the Mo-edges with a lower $\Delta G_{H^*} = 0.08$ eV rather than on the S-edges ($\Delta G_{H^*} = 0.18$ eV),[55] as described in Section 3.1. However, Co incorporation at S-edges can reduce its ΔG_{H^*} to 0.1 eV, while the value at the Mo-edges remains unaffected. As a result, the number of sites with high activity toward hydrogen adsorption increases (Figure 6b).[55] Additionally, the STM image of the chemically synthesized Co promoted MoS_2 (Co-Mo-S) nanoparticle shows that Co incorporation can change the shape of pristine triangular MoS_2 to a truncated hexagonal plane with both Mo and S-Co exposed, which leads to an increase in the length of active edges (Figure 6c).[56] Guided by this fundamental evidence, Merki et al. systemically prepared MoS_3 films doped with Fe, Co, Ni by electrochemical deposition.[57] The promotional effect of Fe, Co, and Ni ions toward HER activity is clearly visible by comparing j_0 and charge-transfer resistance values with those obtained for pristine MoS_3. As predicted by DFT calculations, these ions appear to increase the intrinsic activity of MoS_3 film by interacting with unsaturated S atoms (confirmed by X-ray photoelectron spectroscopy, XPS). The electrochemical experiments further showed that the different promotion effects for Fe, Co, Ni-MoS_3 (Co exhibited the most significant one) were unrelated to Mo content but depended on the nature of metal ions interacted with S atoms.[57]

3.2.3. Origin of the Synergistic Catalysis On Carbon-based Electrocatalysts

In addition to metallic materials, low-dimensional carbon materials (e.g. graphene) as metal-free catalysts, have shown a promising future in various advanced electrolysis applica-

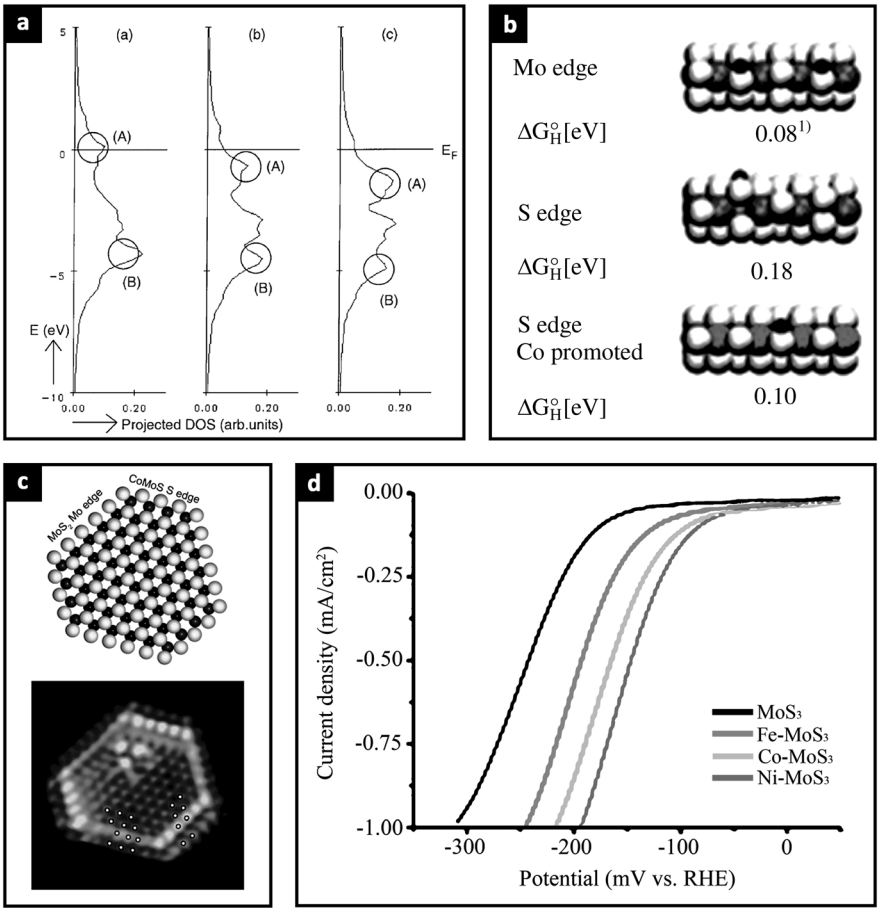

Figure 6. a) The projected DOS for interaction between S 3p states and metal d states in Fe-Mo-S, Co-Mo-S, Ni-Mo-S (from left to right). (A) and (B) indicate the antibonding and bonding orbital, respectively. Reproduced with permission from Ref. [54]. Copyright 1999, Elsevier. b) Differential ΔG_{H^*} of the Mo edge and the S edge in MoS_2 and of the S-Co edge in Co-Mo-S. Reproduced with permission from Ref. [55]. Copyright 2009, RSC. c) Molecular model based on the DFT calculations (top) and atom-resolved STM image of a Co-Mo-S nanocluster (bottom). Reproduced with permission from Ref. [56]. Copyright 2007, Elsevier. (d) HER polarization curves of unpromoted and Fe, Co, Ni-promoted MoS_3 materials in neutral solution. Reproduced with permission from Ref. [57]. Copyright 2012, RSC.

tions.[58] Their abundant sources, variable structures, and tunable chemical composition make them competitive alternatives to (precious) metal counterparts. Intermolecular doping of graphene with heteroatoms, such as nitrogen (N), boron (B), phosphorus (P), fluorine (F), or sulfur (S), is an effective way to tailor its electronic structure and (electro)-chemical properties.[24,59] In particular, the co-doping of two elements which have different electronegativities to that of carbon, for example, B/N,[60] S/N[61] and P/N[7b] couples could lead to a unique electron-donor properties of carbon by the so-called synergistic coupling effect between two heteroatoms. Both experimental tests and theoretical analysis confirmed that such effect could largely boost the electrocatalytic activities of graphene materials toward electrocatalytic ORR and HER.[7b,60,61] Taking N,P co-doped graphene (N,P-G) as an example,[7b] DFT calculations predicted that the N and P heteroatoms could co-activate the adjacent C atom in the graphene matrix by affecting its valence orbital energy levels and leading to a reduced ΔG_{H^*} (Figure 7b). The proof-of-concept experiments indeed showed that the synthesized N,P-G catalyst exhibited a much lower HER overpotential and higher j_0 than those for all investigated pure and single-doped graphene samples (Figure 7a).[7b] Moreover, a good linear trend between theoretical ΔG_{H^*} and measured j_0 is clearly visible (not shown), which also validates the predictive capability of the DFT model for non-metallic systems.

The synergistic effect also occurs in the case of nanocarbon (graphene or carbon nanotubes) and supported metal oxide/hydroxide because of strong coupling between both components.[62] This coupling may induce chemical and/or electrical attachment of catalytically active nanoparticles and conductive nanocarbons, leading to a synergistically enhanced electrocatalytic activity for electrocatalytic ORR,[63] HER,[22,36a] and the oxygen evolution reaction (OER).[64] By the combination of theoretical calculations (e.g. electronic structure analysis and ΔG_{H^*} modelling) and spectroscopic methods (e.g. X-ray absorption near-edge structure), more details can be revealed concerning the origin of this intramolecular synergistic effect. In the case of nitrogen-doped carbon nanotubes with encapsulated iron nanoparticles (Fe@NCNTs), the DFT calculations provide a rigorous theoretical explanation of how metal and N dopants can be used to synergistically optimize ΔG_{H^*}, and consequently, promote the apparent HER activity.[22] In this particular system, the C–H band (sum of C_{2p} and H_{1s}) center is located at a lower energy regime than that on the pristine CNTs, indicating a stronger H–carbon chemical bonding. The electronic structure analysis revealed that this stabilization of H* species may originate from the charge transfer from Fe clusters and N dopants to adjacent carbon atoms, clearly presenting a synergistic effect of Fe and N to co-activate carbon atoms toward HER.[22] In terms of non-metallic systems, graphitic carbon nitride (g-C_3N_4) is a semiconductor and inert electrocatalyst;[65] however, by chemical coupling of g-C_3N_4 with nitrogen-doped graphene sheets (N-graphene), the hybrid (C_3N_4@NG) unexpectedly showed a favorable HER activity, comparable to some of the state-of-the-art metallic materials.[7a] A quantitative indicator of this coupling effect is the measured value of j_0 for the C_3N_4@NG hybrid, which was not only higher than that of g-C_3N_4 and a N-graphene physical mixture but also higher than the summed values obtained for pure g-C_3N_4 and pure N-graphene

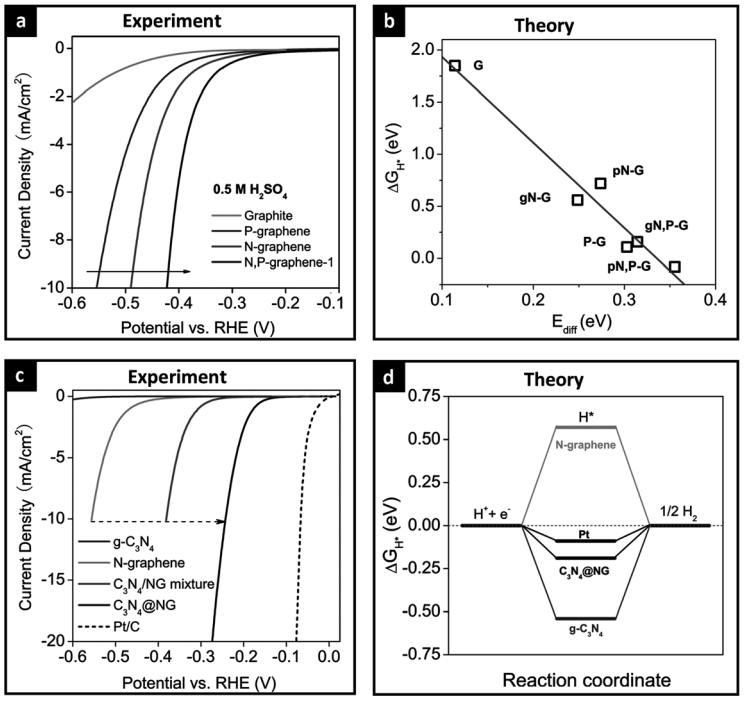

Figure 7. a) HER polarization curves of P and/or N doped graphene electrocatalysts and b) DFT calculated relationship between ΔG_{H^*} and electronic structures for various models. Reproduced with permission from Ref. [7b]. Copyright 2014, ACS. c) HER polarization curves, and d) free-energy diagram of non-metallic electrocatalysts and Pt reference. Reproduced with permission from Ref. [7a]. Copyright 2014, NPG.

components (Figure 7c).[7a] On the theoretical perspective, ΔG_{H^*} values for pure g-C_3N_4 and N-graphene surfaces are opposite in signs, indicating that hydrogen adsorption is either too strong (g-C_3N_4) or too weak (N-graphene).[7a] Chemical coupling of g-C_3N_4 and N-graphene into a uniform hybrid results in a mediated adsorption–desorption behavior ($|\Delta G_{H^*}| \rightarrow 0$), which facilitates the overall HER kinetics (Figure 7d).[7a] Such an atomic-level HER mechanism on the surface of C_3N_4@NG clearly indicates the origin of its strikingly high electrocatalytic activity.

3.3. Evaluating Trends in the Exchange Current

3.3.1. Fundamentals of Volcano Curves

The origin of the "volcano-type" plots in heterogeneous catalysis was first qualitatively described by Sabatier, who pointed out the necessity of appropriate chemical interaction/bonding between reactants and catalyst. If this interaction is too weak, the sluggish reaction-intermediate formation would slowdown the reaction, while if this interaction is too strong, it can block the catalyst's surface and slowdown the reaction.[2b,11] Regarding the electrocatalytic HER, Parsons proposed a volcano-type plot to associate j_0 with the thermodynamically derived ΔG_{H^*} (Figure 8a).[66] The volcano-type plot is observed because according to thermodynamics j_0 can be expressed in terms of $(\theta_H)^{\alpha}(1-\theta_H)^{1-\alpha}$ as a function of ΔG_{H^*} [see Eq. (4)];[4] where α denotes the relative slope of the energy curves of the initial and final states at their point of intersection. The peak of the volcano is reached when $\theta_H = 1-\theta_H = 0.5$ ($\alpha = 1-\alpha = 0.5$), which corresponds to $\Delta G_{H^*} = 0$. The two linear branches of the volcano plot are symmetrical at $\Delta G_{H^*} = 0$: when $\Delta G_{H^*} > 0$ (relatively weak H* adsorption), j_0 exponentially increases with decreasing value of ΔG_{H^*}; when $\Delta G_{H^*} < 0$ (relatively strong H* adsorption), j_0 exponentially decreases with decreasing value of ΔG_{H^*} (Figure 8a).[66]

Guided by Parsons's work, Trasatti presented another form of volcano plot by correlating a wide collection of j_0 values obtained for polycrystalline metal surfaces with the measured hydrogen heats of adsorption (reflecting the strength of M–H bond, as shown in Figure 8b).[67a] Metals, which adsorb hydrogen weakly, such as Ag, Zn, Al, and those that adsorb H strongly, such as Mo, Ta, W, both exhibit low values of j_0. Only metals that show moderate hydrogen adsorption, such as Pt, Pd, and Rh, feature high values of j_0. Trasatti,[67a] Conway and Bockris,[67b] and Kita,[67c] further pointed out that there is a simple phenomenological linear relationship between the logarithm of j_0 and the work function (Φ) for all these metal surfaces. Given that Φ simply depends on the Fermi energy of a metal, there should be some inherent correlation between the electronic properties of metals and their apparent activity as predicted in Section 2.2.2. Nowadays, because of the availability of large computational power, accurate electronic structures of catalysts can be easily explored by DFT. As demonstrated by Nørskov et al., the DFT calculations started to play an increasingly significant role in obtaining ΔG_{H^*} values for the construction of the volcano-type plots for various systems.[12] The DFT modelling has been successfully used for a wide range of different surfaces including metals,[12] alloys,[43a,46] metal carbides,[68] sulfides,[39] and even non-metallic surfaces[7a] that were not characterized by traditional heat of adsorption data. All calculated ΔG_{H^*} values after correlating with the measured j_0 give the volcano-type plots as shown in Figure 8c. As expected, Pt-family metals are located on the peak of the activity volcano with small absolute values of ΔG_{H^*} and large j_0; but some newly developed cost-effective nanostructured catalysts, such as MoS_2 and C_3N_4@NG, show comparable or sometimes better HER activity than traditional metals, as evidenced by both experimental and theoretical evaluations.

3.3.2. Climbing the "Electrocatalytic Activity" Volcano

Given that the theoretical maximum of j_0 is at the peak of the volcano curve with $\Delta G_{H^*} = 0$, climbing the "electrocatalytic activity" volcano is the goal of research on the design and synthesis of highly active catalysts. Because of recent advances in the atomic-level understanding of HER, many new electrocatalysts with carefully controlled architectures and optimized electronic properties, such as a pseudomorphic Pd monolayer on a single-crystal PtRu substrate[43a] and BiPt surface alloys,[46] showed even better HER activity than pure Pt catalysts. In addition to HER, the electrocatalytic activity trends can also be evaluated by using analogous volcano-type plots for various electrochemical processes, such as OER (standard free energy of HO* oxidation, $\Delta G_{O^*} - \Delta G_{HO^*}$, as shown in Figure 8d),[69] ORR (O* intermediate binding energy, E_{O^*}, as shown in Figure 8e),[24,48c,70] CO_2 reduction (descriptor depends on the reaction mechanism and pathway),[71] and electrochemical H_2O_2 production (HOO* adsorption energy, ΔG_{HOO^*}, as shown in Figure 8f).[49] All of the descriptors used showed good correlations with experimental activity data. More importantly, these fundamental descriptors provide a powerful tool for predicting the electrocatalytic activity trends, allowing the design and synthesis of advanced electrocatalysts for various energy-relevant processes that perform better than traditional ones.[24,49b]

4. Outlook and Future Challenges

Although great progress have been made in the design of highly efficient HER electrocatalysts by combining the currently available computational and experimental methods, there are still several issues that are not solved yet by this promising strategy. First, the DFT methodology is still under development toward accurately describing relatively complex systems under real HER conditions. For example, in the most important case of the aforementioned DFT-derived volcano plots, the value of the calculated ΔG_{H^*} is based on H_{UPD} while j_0 might correspond to weakly adsorbed H_{OPD}.[10] This is also demonstrated by the disagreement between the measured M–H bond strength and ΔG_{H^*} on Co and Ni surfaces.[72] Secondly, although the correlation between j_0 and ΔG_{H^*} is appealing, this model is still over simplistic and some important effects are disregarded, such as the double layer and solvation effects.[72] Nørskov et al. calculated the electrical field effect

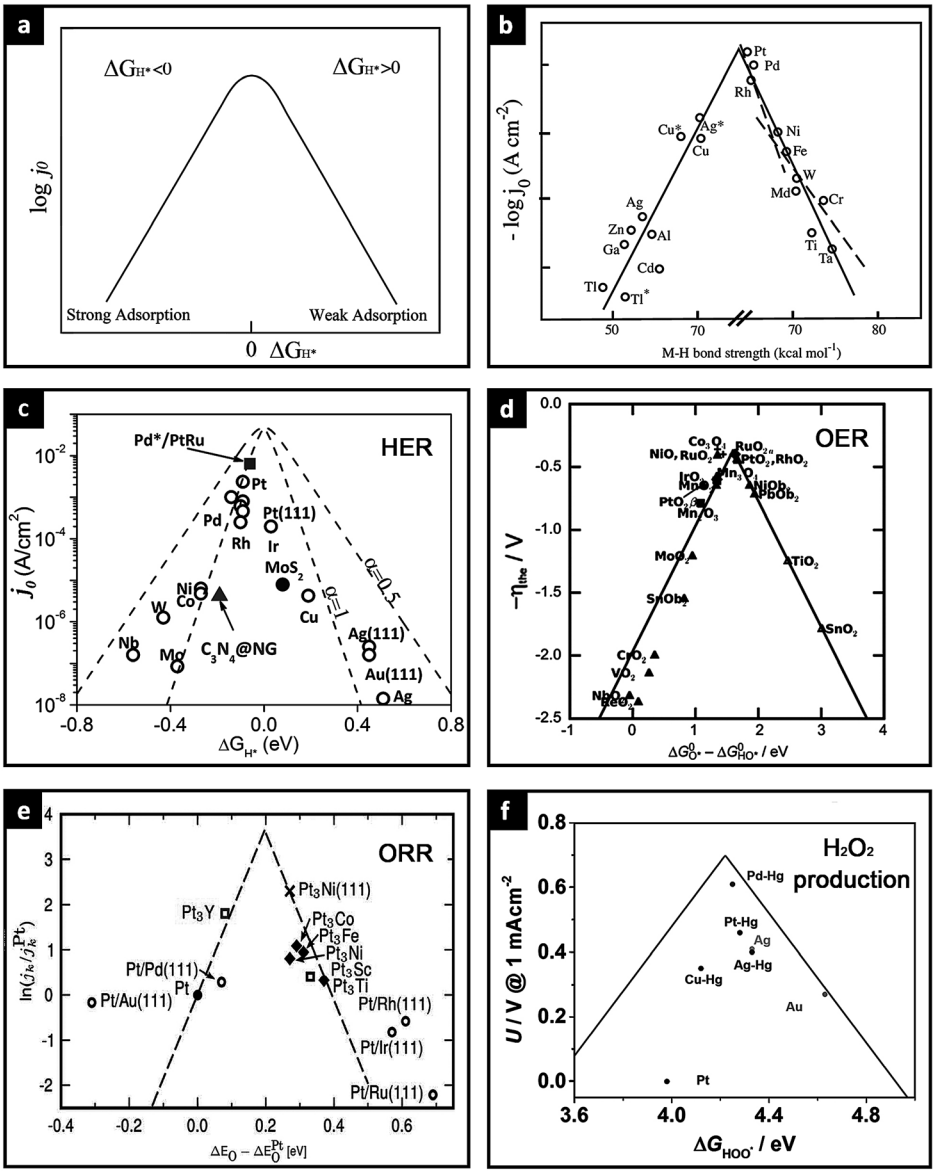

Figure 8. a) Relationship between j_0 and ΔG_{H^*} under assumption of a Langmuir adsorption model. b) Electrochemically measured j_0 values on metals versus the strength of metal–hydrogen bond derived from the heat of hydride formation. Reproduced with permission from Ref. [2b], data were adapted from Ref. [67a]. Copyright 2011, John Wiley and Sons. c) Dependence of j_0 on ΔG_{H^*} for HER on the surface of various metals, alloy compounds, and non-metallic materials. Data are collected from Refs. [7a, 12, 28, 43a]. d) Activity trends towards OER as a function of the standard free energy of HO* oxidation ($\Delta G_{O^*} - \Delta G_{HO^*}$) for rutile and anatase oxides. Reproduced with permission from Ref. [69]. Copyright 2011, Wiley-VCH. (e) ORR kinetic current density (j_k) for a range of alloy electrocatalysts with Pt "skins" plotted as a function of the oxygen adsorption energy (ΔE_{O^*}). All data are shown relative to Pt. Reproduced with permission from Ref. [48c]. Copyright 2009, NPG. (f) Potential required to reach 1 mA cm^{-2} of H_2O_2 production kinetic current density on polycrystalline catalysts as a function of the calculated HOO* binding energy (ΔG_{HOO^*}). Reproduced with permission from Ref. [49a]. Copyright 2014, ACS.

for OH* adsorption on a Pt surface to be 0.015 eV under a potential bias of 1 V,[70] but such an effect has not been analyzed within the HER Scheme yet. Although the calculation of ΔG_{H^*} in vacuum could fundamentally meet the requirements for better screening of HER electrocatalysts, a full consideration of all experimental parameters and variables in one calculation scheme would be scientifically interesting. Finally, the DFT theory is powerful only for modelling the single-crystal surfaces, while it is well-known that the most developed promising metallic nanoparticles are covered with different facets, whose surface percentages vary with particle size and shape.[73] Clearly, the HER activity descriptors, such as ΔG_{H^*}, on each face and $H_{OPD/UPD}$ coverage are totally different.[8,21] Therefore, the construction of polycrystalline surface models remains a challenge owing to both the lack of sufficient experimental evidence and the large size of unit cells for which computations must be carried out.

The promising non-metallic carbon-based electrocatalysts have demonstrated competitive properties as the next gen-

eration of highly efficient HER catalysts. Fortunately, the DFT computations showed their powerful predicting capability for these materials, paving the way toward molecular design of catalysts for HER. A combination of theoretical calculations and experimental data provides clear and solid evidence that, similarly to precious metals, their well-designed metal-free counterparts have also a great potential for highly efficient electrocatalytic HER, thus will largely expand the spectrum of electrocatalysts for HER and other energy-related electrocatalytic reactions.

We gratefully acknowledge the financial support by Australian Research Council (ARC) through the Discovery Project programs (DP140104062 and DP130104459).

Received: July 9, 2014
Published online: November 10, 2014

[1] a) N. S. Lewis, D. G. Nocera, *Proc. Natl. Acad. Sci. USA* **2006**, *103*, 15729 – 15735; b) R. Borup, J. Meyers, B. Pivovar, Y. S. Kim, R. Mukundan, N. Garland, D. Myers, M. Wilson, F. Garzon, D. Wood, P. Zelenay, K. More, K. Stroh, T. Zawodzinski, J. Boncella, J. E. McGrath, M. Inaba, K. Miyatake, M. Hori, K. Ota, Z. Ogumi, S. Miyata, A. Nishikata, Z. Siroma, Y. Uchimoto, K. Yasuda, K. Kimijima, N. Iwashita, *Chem. Rev.* **2007**, *107*, 3904 – 3951.

[2] a) M. W. Breiter in *Handbook of Fuel Cells* (Eds.: W. Vielstich, H. A. Gasteiger, A. Lamm, H. Yokokawa), Wiley, **2010**; b) R. Parsons in *Catalysis in Electrochemistry* (Eds.: E. Santos, W. Schmickler), Wiley, **2011**, Chap. 1, pp. 1 – 15.

[3] a) L. A. Kibler, *ChemPhysChem* **2006**, *7*, 985 – 991; b) J. K. Nørskov, T. Bligaard, J. Rossmeisl, C. H. Christensen, *Nat. Chem.* **2009**, *1*, 37 – 46; c) N. M. Marković in *Handbook of Fuel Cells* (Eds.: W. Vielstich, H. A. Gasteiger, A. Lamm, H. Yokokawa), Wiley, **2010**; d) J. Greeley, N. M. Marković, *Energy Environ. Sci.* **2012**, *5*, 9246 – 9256.

[4] B. E. Conway, B. V. Tilak, *Electrochim. Acta* **2002**, *47*, 3571 – 3594.

[5] a) M. G. Walter, E. L. Warren, J. R. McKone, S. W. Boettcher, Q. Mi, E. A. Santori, N. S. Lewis, *Chem. Rev.* **2010**, *110*, 6446 – 6473; b) J. R. McKone, S. C. Marinescu, B. S. Brunschwig, J. R. Winkler, H. B. Gray, *Chem. Sci.* **2014**, *5*, 865 – 878.

[6] a) C. G. Morales-Guio, L. Stern, X. Hu, *Chem. Soc. Rev.* **2014**, *43*, 6555 – 6569; b) J. Yang, H. S. Shin, *J. Mater. Chem. A* **2014**, *2*, 5979 – 5985; c) Y. Yan, B. Xia, Z. Xu, X. Wang, *ACS Catal.* **2014**, *4*, 1693 – 1705.

[7] a) Y. Zheng, Y. Jiao, Y. Zhu, L. H. Li, Y. Han, Y. Chen, A. Du, M. Jaroniec, S. Z. Qiao, *Nat. Commun.* **2014**, *5*, 3783; b) Y. Zheng, Y. Jiao, L. H. Li, T. Xing, Y. Chen, M. Jaroniec, S. Z. Qiao, *ACS Nano* **2014**, *8*, 5290 – 5296.

[8] N. M. Marković, P. N. Ross, Jr., *Surf. Sci. Rep.* **2002**, *45*, 117 – 229.

[9] H. Wolfschmidt, O. Paschos, U. Stimming, *Fuel Cell Science* (Eds.: A. Wieckowski, J. Nørskov), Wiley, **2010**, Chap. 1, pp. 1 – 70.

[10] A. Lasia in *Handbook of Fuel Cells* (Eds.: W. Vielstich, H. A. Gasteiger, A. Lamm, H. Yokokawa), Wiley, **2010**.

[11] P. Sabatier, La catalyse en chimie organique, **1920**.

[12] J. K. Nørskov, T. Bligaard, A. Logadottir, J. R. Kitchin, J. G. Chen, S. Pandelov, U. Stimming, *J. Electrochem. Soc.* **2005**, *152*, J23 – J26.

[13] A. J. Bard, L. R. Faulkner, *Electrochemical Methods*: *Fundamentals and Applications*, Wiley, **2000**.

[14] D. S. Sholl, J. A. Steckel, *Density Functional Theory*, Wiley, **2009**, pp. 113 – 130.

[15] A. Nilsson, L. G. M. Pettersson, B. Hammer, T. Bligaard, C. H. Christensen, J. K. Nørskov, *Catal. Lett.* **2005**, *100*, 111 – 114.

[16] a) E. Santos, W. Schmickler, *ChemPhysChem* **2006**, *7*, 2282 – 2285; b) E. Santos, A. Lundin, K. Pötting, P. Quaino, W. Schmickler, *Phys. Rev. B* **2009**, *79*, 235436.

[17] B. Hammer, J. K. Nørskov, *Nature* **1995**, *376*, 238 – 240.

[18] D. S. Su, J. Zhang, B. Frank, A. Thomas, X. Wang, J. Paraknowitsch, R. Schlögl, *ChemSusChem* **2010**, *3*, 169 – 180.

[19] Z. Ao, S. Li, *Graphene Simulation* (Ed.: J. Gong), InTech, **2011**, pp. 53 – 74.

[20] a) I. Pasti, S. Mentus, *Phys. Chem. Chem. Phys.* **2009**, *11*, 6225 – 6233; b) C. Zhang, X. Chen, H. Lin, *J. Phys. Condens. Matter* **2012**, *24*, 035701.

[21] a) E. Skúlason, V. Tripkovic, M. E. Björketun, S. d. Gudmundsdóttir, G. Karlberg, J. Rossmeisl, T. Bligaard, H. Jónsson, J. K. Nørskov, *J. Phys. Chem. C* **2010**, *114*, 18182 – 18197; b) J. Rossmeisl, E. Skúlason, M. E. Björketun, V. Tripkovic, J. K. Nørskov, *Chem. Phys. Lett.* **2008**, *466*, 68 – 71.

[22] J. Deng, P. Ren, D. Deng, L. Yu, F. Yang, X. Bao, *Energy Environ. Sci.* **2014**, *7*, 1919 – 1923.

[23] E. Skúlason, G. S. Karlberg, J. Rossmeisl, T. Bligaard, J. Greeley, H. Jónsson, J. K. Nørskov, *Phys. Chem. Chem. Phys.* **2007**, *9*, 3241 – 3250.

[24] Y. Jiao, Y. Zheng, M. Jaroniec, S. Z. Qiao, *J. Am. Chem. Soc.* **2014**, *136*, 4394 – 4403.

[25] a) N. M. Marković, S. T. Sarraf, H. A. Gasteriger, P. N. Ross, Jr., *J. Chem. Soc. Faraday Trans.* **1996**, *92*, 3719 – 3725; b) N. M. Marković, B. N. Grgur, P. N. Ross, Jr., *J. Phys. Chem. B* **1997**, *101*, 5405 – 5413; c) J. Barber, S. Morin, B. E. Conway, *J. Electroanal. Chem.* **1998**, *446*, 125 – 138; d) J. Barber, B. E. Conway, *J. Electroanal. Chem.* **1999**, *461*, 80 – 89; e) F. Yang, Q. Zhang, Y. Liu, S. Chen, *J. Phys. Chem. B* **2011**, *115*, 19311 – 19319.

[26] H. Tributsch, J. C. Bennett, *J. Electroanal. Chem.* **1977**, *81*, 97 – 111.

[27] B. Hinnemann, P. G. Moses, J. Bonde, K. P. Jørgensen, J. H. Nielsen, S. Horch, I. Chorkendorff, J. K. Nørskov, *J. Am. Chem. Soc.* **2005**, *127*, 5308 – 5309.

[28] T. F. Jaramillo, K. P. Jørgensen, J. Bonde, J. H. Nielsen, S. Horch, I. Chorkendorff, *Science* **2007**, *317*, 100 – 102.

[29] J. Kibsgaard, Z. Chen, B. N. Reinecke, T. F. Jaramillo, *Nat. Mater.* **2012**, *11*, 963 – 969.

[30] Z. Chen, D. Cummins, B. N. Reinecke, E. Clark, M. K. Sunkara, T. F. Jaramillo, *Nano Lett.* **2011**, *11*, 4168 – 4175.

[31] a) Z. Lu, H. Zhang, W. Zhu, X. Yu, Y. Kuang, Z. Chang, X. Lei, X. Sun, *Chem. Commun.* **2013**, *49*, 7516 – 7518; b) X. Ge, L. Chen, L. Zhang, Y. Wen, A. Hirata, M. Chen, *Adv. Mater.* **2014**, *26*, 3100 – 3104.

[32] X. Zheng, J. Xu, K. Yan, H. Wang, Z. Wang, S. Yang, *Chem. Mater.* **2014**, *26*, 2344 – 2353.

[33] a) H. Vrubel, D. Merki, X. Hu, *Energy Environ. Sci.* **2012**, *5*, 6136 – 6144; b) H. Wang, Z. Lu, D. Kong, J. Sun, T. M. Hymel, Y. Cui, *ACS Nano* **2014**, *8*, 4940 – 4947.

[34] M. A. Lukowski, A. S. Daniel, F. Meng, A. Forticaux, L. Li, S. Jin, *J. Am. Chem. Soc.* **2013**, *135*, 10274 – 10277.

[35] D. Voiry, H. Yamaguchi, J. Li, R. Silva, D. C. B. Alves, T. Fujita, M. Chen, T. Asefa, V. B. Shenoy, G. Eda, M. Chhowalla, *Nat. Mater.* **2013**, *12*, 850 – 855.

[36] a) Y. Li, H. Wang, L. Xie, Y. Liang, G. Hong, H. Dai, *J. Am. Chem. Soc.* **2011**, *133*, 7296 – 7299; b) A. J. Smith, Y. H. Chang, K. Raidongia, T. Y. Chen, L. J. Li, J. Huang, *Adv. Energy Mater.* **2014**, DOI: 10.1002/aenm.201400398.

[37] D. J. Li, U. N. Maiti, J. Lim, D. S. Choi, W. J. Lee, Y. Oh, G. Y. Lee, S. O. Kim, *Nano Lett.* **2014**, *14*, 1228 – 1233.

[38] D. H. Youn, S. Han, J. Y. Kim, J. Y. Kim, H. Park, S. H. Choi, J. S. Lee, *ACS Nano* **2014**, *8*, 5164 – 5173.

[39] C. Tsai, F. Abild-Pedersen, J. K. Nørskov, *Nano Lett.* **2014**, *14*, 1381 – 1387.
[40] J. Xie, H. Zhang, S. Li, R. Wang, X. Sun, M. Zhou, J. Zhou, X. W. Lou, Y. Xie, *Adv. Mater.* **2013**, *25*, 5807 – 5813.
[41] J. Xie, J. Zhang, S. Li, F. Grote, X. Zhang, H. Zhang, R. Wang, Y. Lei, B. Pan, Y. Xie, *J. Am. Chem. Soc.* **2013**, *135*, 17881 – 17888.
[42] a) B. Hammer, J. K. Nørskov, *Advances in Catalysis*, *Vol. 45* (Eds.: H. K. Bruce, C. Gates), Academic Press, **2000**, pp. 71 – 129; b) J. K. Nørskov, F. Abild-Pedersen, F. Studt, T. Bligaard, *Proc. Natl. Acad. Sci. USA* **2011**, *108*, 937 – 943; c) J. K. Norskov, T. Bligaard, B. Hvolbaek, F. Abild-Pedersen, I. Chorkendorff, C. H. Christensen, *Chem. Soc. Rev.* **2008**, *37*, 2163 – 2171.
[43] a) J. Greeley, J. K. Nørskov, L. A. Kibler, A. M. El-Aziz, D. M. Kolb, *ChemPhysChem* **2006**, *7*, 1032 – 1035; b) T. Hofmann, T. H. Yu, M. Folse, L. Weinhardt, M. Bär, Y. Zhang, B. V. Merinov, D. J. Myers, W. A. Goddard, C. Heske, *J. Phys. Chem. C* **2012**, *116*, 24016 – 24026; c) B. S. Mun, C. Lee, V. Stamenkovic, N. M. Marković, P. N. Ross, *Phys. Rev. B* **2005**, *71*, 115420; d) A. Baraldi, S. Lizzit, G. Comelli, M. Kiskinova, R. Rosei, K. Honkala, J. K. Nørskov, *Phys. Rev. Lett.* **2004**, *93*, 046101.
[44] a) J. Rodriguez, *Surf. Sci. Rep.* **1996**, *24*, 223 – 287; b) J. G. Chen, C. A. Menning, M. B. Zellner, *Surf. Sci. Rep.* **2008**, *63*, 201 – 254.
[45] J. R. Kitchin, J. K. Nørskov, M. A. Barteau, J. G. Chen, *Phys. Rev. Lett.* **2004**, *93*, 156801.
[46] J. Greeley, T. F. Jaramillo, J. Bonde, I. Chorkendorff, J. K. Nørskov, *Nat. Mater.* **2006**, *5*, 909 – 913.
[47] M. E. Björketun, A. S. Bondarenko, B. L. Abrams, I. Chorkendorff, J. Rossmeisl, *Phys. Chem. Chem. Phys.* **2010**, *12*, 10536 – 10541.
[48] a) V. R. Stamenkovic, B. Fowler, B. S. Mun, G. Wang, P. N. Ross, C. A. Lucas, N. M. Marković, *Science* **2007**, *315*, 493 – 497; b) V. R. Stamenkovic, B. S. Mun, M. Arenz, K. J. J. Mayrhofer, C. A. Lucas, G. Wang, P. N. Ross, N. M. Marković, *Nat. Mater.* **2007**, *6*, 241 – 247; c) J. Greeley, I. E. L. Stephens, A. S. Bondarenko, T. P. Johansson, H. A. Hansen, T. F. Jaramillo, J. Rossmeisl, I. Chorkendorff, J. K. Nørskov, *Nat. Chem.* **2009**, *1*, 552 – 556.
[49] a) A. Verdaguer-Casadevall, D. Deiana, M. Karamad, S. Siahrostami, P. Malacrida, T. W. Hansen, J. Rossmeisl, I. Chorkendorff, I. E. L. Stephens, *Nano Lett.* **2014**, *14*, 1603 – 1608; b) S. Siahrostami, A. Verdaguer-Casadevall, M. Karamad, D. Deiana, P. Malacrida, B. Wickman, M. Escudero-Escribano, E. A. Paoli, R. Frydendal, T. W. Hansen, I. Chorkendorff, I. E. L. Stephens, J. Rossmeisl, *Nat. Mater.* **2013**, *12*, 1137 – 1143.
[50] B. Hammer, J. K. Nørskov, *Surf. Sci.* **1995**, *343*, 211 – 220.
[51] L. A. Kibler, A. M. El-Aziz, R. Hoyer, D. M. Kolb, *Angew. Chem. Int. Ed.* **2005**, *44*, 2080 – 2084; *Angew. Chem.* **2005**, *117*, 2116 – 2120.
[52] T. A. Maark, A. A. Peterson, *J. Phys. Chem. C* **2014**, *118*, 4275 – 4281.
[53] a) F. Besenbacher, M. Brorson, B. S. Clausen, S. Helveg, B. Hinnemann, J. Kibsgaard, J. V. Lauritsen, P. G. Moses, J. K. Nørskov, H. Topsøe, *Catal. Today* **2008**, *130*, 86 – 96; b) J. V. Lauritsen, S. Helveg, E. Lægsgaard, I. Stensgaard, B. S. Clausen, H. Topsøe, F. Besenbacher, *J. Catal.* **2001**, *197*, 1 – 5.
[54] L. S. Byskov, J. K. Nørskov, B. S. Clausen, H. Topsøe, *J. Catal.* **1999**, *187*, 109 – 122.
[55] J. Bonde, P. G. Moses, T. F. Jaramillo, J. K. Nørskov, I. Chorkendorff, *Faraday Discuss.* **2009**, *140*, 219 – 231.
[56] J. V. Lauritsen, J. Kibsgaard, G. H. Olesen, P. G. Moses, B. Hinnemann, S. Helveg, J. K. Nørskov, B. S. Clausen, H. Topsøe, E. Lægsgaard, F. Besenbacher, *J. Catal.* **2007**, *249*, 220 – 233.
[57] D. Merki, H. Vrubel, L. Rovelli, S. Fierro, X. Hu, *Chem. Sci.* **2012**, *3*, 2515 – 2525.
[58] a) Y. Sun, Q. Wu, G. Shi, *Energy Environ. Sci.* **2011**, *4*, 1113 – 1132; b) L. Dai, D. W. Chang, J.-B. Baek, W. Lu, *Small* **2012**, *8*, 1130 – 1166; c) D. Chen, L. Tang, J. Li, *Chem. Soc. Rev.* **2010**, *39*, 3157 – 3180; d) H. Wang, T. Maiyalagan, X. Wang, *ACS Catal.* **2012**, *2*, 781 – 794.
[59] a) Y. Zheng, Y. Jiao, M. Jaroniec, Y. Jin, S. Z. Qiao, *Small* **2012**, *8*, 3550 – 3566; b) J. P. Paraknowitsch, A. Thomas, *Energy Environ. Sci.* **2013**, *6*, 2839 – 2855; c) D. W. Wang, D. Su, *Energy Environ. Sci.* **2014**, *7*, 576 – 591.
[60] Y. Zheng, Y. Jiao, L. Ge, M. Jaroniec, S. Z. Qiao, *Angew. Chem. Int. Ed.* **2013**, *52*, 3110 – 3116; *Angew. Chem.* **2013**, *125*, 3192 – 3198.
[61] J. Liang, Y. Jiao, M. Jaroniec, S. Z. Qiao, *Angew. Chem. Int. Ed.* **2012**, *51*, 11496 – 11500; *Angew. Chem.* **2012**, *124*, 11664 – 11668.
[62] Y. Liang, Y. Li, H. Wang, H. Dai, *J. Am. Chem. Soc.* **2013**, *135*, 2013 – 2036.
[63] a) Y. Liang, Y. Li, H. Wang, J. Zhou, J. Wang, T. Regier, H. Dai, *Nat. Mater.* **2011**, *10*, 780 – 786; b) D. Deng, L. Yu, X. Chen, G. Wang, L. Jin, X. Pan, J. Deng, G. Sun, X. Bao, *Angew. Chem. Int. Ed.* **2013**, *52*, 371 – 375; *Angew. Chem.* **2013**, *125*, 389 – 393.
[64] M. Gong, Y. Li, H. Wang, Y. Liang, J. Z. Wu, J. Zhou, J. Wang, T. Regier, F. Wei, H. Dai, *J. Am. Chem. Soc.* **2013**, *135*, 8452 – 8455.
[65] a) Y. Zheng, J. Liu, J. Liang, M. Jaroniec, S. Z. Qiao, *Energy Environ. Sci.* **2012**, *5*, 6717 – 6731; b) A. Thomas, A. Fischer, F. Goettmann, M. Antonietti, J.-O. Müller, R. Schlögl, J. M. Carlsson, *J. Mater. Chem.* **2008**, *18*, 4893 – 4908; c) Y. Zheng, Y. Jiao, J. Chen, J. Liu, J. Liang, A. Du, W. Zhang, Z. Zhu, S. C. Smith, M. Jaroniec, G. Q. Lu, S. Z. Qiao, *J. Am. Chem. Soc.* **2011**, *133*, 20116 – 20119.
[66] R. Parsons, *Trans. Faraday Soc.* **1958**, *54*, 1053 – 1063.
[67] a) S. Trasatti, *J. Electroanal. Chem.* **1972**, *39*, 163 – 184; b) B. E. Conway, J. O. Bockris, *J. Chem. Phys.* **1957**, *26*, 532; c) H. Kita, *J. Electrochem. Soc.* **1966**, *113*, 289 – 290.
[68] a) R. Michalsky, Y.-J. Zhang, A. A. Peterson, *ACS Catal.* **2014**, *4*, 1274 – 1278; b) D. V. Esposito, S. T. Hunt, Y. C. Kimmel, J. G. Chen, *J. Am. Chem. Soc.* **2012**, *134*, 3025 – 3033.
[69] I. C. Man, H.-Y. Su, F. Calle-Vallejo, H. A. Hansen, J. I. Martínez, N. G. Inoglu, J. Kitchin, T. F. Jaramillo, J. K. Nørskov, J. Rossmeisl, *ChemCatChem* **2011**, *3*, 1159 – 1165.
[70] J. K. Nørskov, J. Rossmeisl, A. Logadottir, L. Lindqvist, J. R. Kitchin, T. Bligaard, H. Jónsson, *J. Phys. Chem. B* **2004**, *108*, 17886 – 17892.
[71] a) V. Tripkovic, M. Vanin, M. Karamad, M. E. Björketun, K. W. Jacobsen, K. S. Thygesen, J. Rossmeisl, *J. Phys. Chem. C* **2013**, *117*, 9187 – 9195; b) A. A. Peterson, J. K. Nørskov, *J. Phys. Chem. Lett.* **2012**, *3*, 251 – 258.
[72] W. Schmickler, S. Trasatti, *J. Electrochem. Soc.* **2006**, *153*, L31 – L32.
[73] S. E. F. Kleijn, S. C. S. Lai, M. T. M. Koper, P. R. Unwin, *Angew. Chem. Int. Ed.* **2014**, *53*, 3558 – 3586; *Angew. Chem.* **2014**, *126*, 3630 – 3660.